Effect of sink strength dispersion on cluster size distributions simulated by cluster dynamics

Denise Carpentier, Thomas Jourdan, Pierre Terrier, Manuel Athenes, Yann Le Bouar

Effect of sink strength dispersion on cluster size distributions simulated by cluster dynamics

D. Carpentier[a], T. Jourdan[a,*], P. Terrier[a,b], M. Athènes[a], Y. Le Bouar[c]

[a] *DEN-Service de Recherches de Métallurgie Physique, CEA, Université Paris-Saclay, F-91191, Gif-sur-Yvette, France*
[b] *Université Paris-Est, CERMICS (ENPC), INRIA, F-77455 Marne-la-Vallée, France*
[c] *LEM, Université Paris-Saclay, ONERA, CNRS, 29 av. de la division Leclerc, 92322 Châtillon, France*

Abstract

The microstructure evolution in irradiated materials can be conveniently modelled, at large scale, by cluster dynamics (CD). In this approach, the effect of the local environment of defect clusters is neglected. In this article, we first check the validity of this assumption by comparing CD to object kinetic Monte Carlo (OKMC) simulations. We show that for microstructures produced under irradiation, taking into account in CD only the average dependency of clusters' growth rate on volume fraction does not permit to reproduce reference OKMC results. Accordingly, the sink strength dispersion, quantified using OKMC, is introduced in CD, using a new formalism depending on the Voronoi volumes of defect clusters. CD calculations including sink strength dispersion are shown to be in better agreement with reference OKMC simulations and experimental observations than are classical CD calculations.

Keywords: Cluster dynamics ; object kinetic Monte Carlo; diffusional interactions; spatial correlations

1. Introduction

Long term evolution of microstructures containing second phase particles or defect clusters can be efficiently simulated by cluster dynamics (CD). Its raw

*Corresponding author
Email address: thomas.jourdan@cea.fr (T. Jourdan)

output consists in size distributions at a desired time, and this approach can be applied, for example, to the description of precipitates [1, 2, 3], voids and dislocation loops [4, 5, 6]. Its mean field character makes it particularly efficient compared to other methods which describe the position of clusters and thus take into account spatial correlations naturally, such as atomistic and object kinetic Monte Carlo (A/OKMC) methods. Under thermal aging, CD reproduces well AKMC results provided it is carefully parametrized with the same atomistic data [2, 3] and that potential corrections are added to the classical formalism to handle concentrated alloys [7, 8]. For materials under irradiation, it has been shown that provided input parameters in CD and OKMC are consistent, cluster size distributions are very similar for low volume fractions, even if distributions obtained with OKMC can be slightly broader than those obtained with CD [9]. Tests at higher volume fractions have not been performed, to our knowledge. Comparison of CD and experimental results show that the mean field approach becomes less precise at larger dose, the experimental distributions being broader [4].

Such discrepancies in particle size distributions have been extensively studied in the context of Ostwald ripening [10]. Indeed it is known that experimental distributions can be broader than the prediction of Lifshitz-Slyozov-Wagner (LSW) theory, which is itself in overall good agreement with CD [2]. LSW approach and CD in its simplest form both neglect the effect of volume fraction of particles. However, the diffusion field around a particle can be modified by the presence of other particles in the surroundings, thereby modifying the growth rate of the particle [11, 12]. For Ostwald ripening, numerous attempts have been made to determine the *average* growth rate of particles, taking into account the presence of other particles [10]. The dependency of the average growth rate of particles on volume fraction can be rationalized in terms of microstructure-dependent "sink strengths" [13]. Such dependency has been early recognized in the simulation of radiation-induced clusters such as voids and dislocation loops [14]. However, CD calculations with sink strengths depending on the volume fraction of second phase particles remain rather scarce [2, 15]. Beyond the

effect on the average growth rate, the variety of local environments of particles can lead to a *dispersion* of sink strengths for a given particle size. This dispersion is neglected in CD and to our knowledge, the validity of this assumption has never been checked.

In this article we investigate the effect of local neighborhood on the sink strengths of dislocation loops in microstructures generated by OKMC. We show that using the average growth rate for a given cluster size in CD is not sufficient to reproduce reference cluster distributions determined by OKMC. It is therefore necessary to introduce explicitly the sink strength dispersion in CD due to the neighborhood effects. For this purpose, a simple sink strength expression is proposed, which reproduces the dispersion. The CD formalism is modified to introduce the sink strength dispersion.

The paper is organized as follows. In section 2, we start by describing the method used to generate microstructures in OKMC simulations, and to calculate the sink strengths in these microstructures. By comparing microstructures produced by equivalent OKMC and CD simulations, volume fraction effects and the influence of sink strength dispersion are quantified. Then a sink strength expression is derived in section 3 to reproduce the dispersion obtained in microstructures. In section 4, we present a new method to introduce the sink strength dispersion in CD. Extension of the method to more complicated cases, in particular if elastic interactions between sinks and point defects are considered, is discussed in section 5. This model is then used to simulate electron irradiation experiments performed on aluminum thin foils (section 6).

2. Volume fraction effects and sink strength dispersion in microstructures

In order to quantify the sink strength dispersion and show its link with neighborhood effects, sink strengths are evaluated in dislocation loop microstructures using OKMC. To consider microstructures as realistic as possible, the formation of dislocation loops by agglomeration of self-interstitial atoms (SIAs) is also

simulated by OKMC. Cluster distributions thus obtained can be compared to distributions given by equivalent CD calculations, relying on some classical sink strength expressions which describe volume fraction effects at different levels of accuracy. This enables us to quantify the effect of non-zero volume fraction and sink strength dispersion on cluster distributions.

2.1. Creation of microstructures

The microstructures are created by OKMC simulations [16, 17], starting from a simulation box containing no defects. SIAs are introduced with a given creation rate G. They migrate by atomic jumps until reacting with another SIA, thus creating a dislocation loop, or with a loop. We consider immobile Frank loops in $\{111\}$ planes with Burgers vector $\boldsymbol{b}$ of type $1/3\langle 111\rangle$. The orientation is randomly chosen among the four variants when the loops are created.

Two models are considered for the absorption of SIAs. In the simplest model, which is studied in detail in this article, an SIA is absorbed by a loop containing n SIAs when it enters the sphere which encloses the loop, *i. e.* if the distance d between the loop center and the SIA verifies

$$d \leq r_{\mathrm{L},n} + r_{\mathrm{PD}}, \tag{1}$$

where r_{PD} is the point defect radius, set to the atomic radius, and $r_{\mathrm{L},n}$ is the loop radius. The loop radius is related to n through

$$r_{\mathrm{L},n} = \sqrt{\frac{nV_{\mathrm{at}}}{\pi b}}, \tag{2}$$

with V_{at} the atomic volume and b the norm of the Burgers vector. We also assume that SIAs do not interact elastically with the sink. The choice of the absorption on an encapsulating sphere instead of a torus, without elastic interactions, enables us to use CD with a larger number of sink strength expressions.

In section 5, we consider a more realistic model. Absorption of SIAs by loops occurs on the torus of radius r_{L} and pipe radius $r_{\mathrm{p}} = 2b$. This means that a point defect is absorbed by the loop when the distance d between the point

defect and the dislocation line verifies

$$d \leq r_{\mathrm{p}} + r_{\mathrm{PD}}. \tag{3}$$

Some calculations have been performed with elastic interactions in this case.

In OKMC simulations, the computation time increases with the number of defects. To decrease the computation time, one way is to reduce the box size as much as possible. However, two difficulties can arise. The first one is related to the potentially large fluctuations of cluster distributions from one simulation to another, due to the moderate number of clusters. To obtain well-converged cluster distributions, we average cluster distributions over a large number of independent simulations. In this study, approximately a thousand of simulations are used. The second problem is that the limited box size can itself lead to a distortion in the cluster distribution. Indeed, in insufficiently large boxes, a single cluster rapidly absorbs all the migrating point defects and remains alone. Moreover, the periodic boundary conditions force the point defects to interact with each other or with the remaining cluster. Therefore clusters can become abnormally large and final cluster size distributions, obtained by averaging over several simulations, vary with the box size for too small boxes. An example is given in Fig. 1, with boxes of side length $l = 50\,\mathrm{nm}$, $l = 100\,\mathrm{nm}$ and $l = 200\,\mathrm{nm}$, a creation rate $G = 10^{-1}\,\mathrm{dpa.s}^{-1}$ and a physical time $t = 10^{-3}$ s. It can be seen that the smallest box size gives an inconsistent distribution, while the box sizes $l = 100\,\mathrm{nm}$ and $l = 200\,\mathrm{nm}$ give similar results. The convergence has been checked for all the studied cases and sufficiently large boxes have been chosen.

In this work we have considered three different creation rates: 10^{-3} dpa.s^{-1}, 10^{-2} dpa.s^{-1} and 10^{-1} dpa.s^{-1}. We only report the results for $G = 10^{-1}$ dpa.s^{-1}, since similar results are obtained for the other dose rates. The case $G = 10^{-3}$ dpa.s^{-1} can be found in the Supplementary Material and all results are available in Ref. [18]. The high creation rates considered here and in the rest of this work are to simulate high doses with the short simulation times accessible with the OKMC simulations. Other parameters are provided in Table 1. Given the low temperature and high binding energies of clusters [19], thermal emission

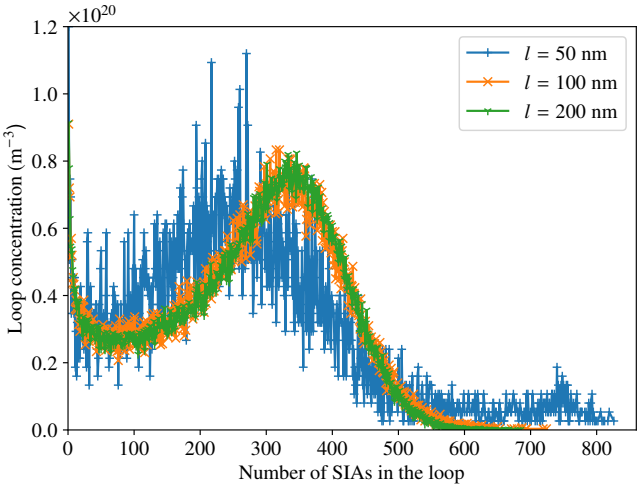

Figure 1: Example of cluster size distributions obtained with OKMC simulations, with $G = 10^{-1}$ dpa.s^{-1}, $t = 10^{-3}$ s and with the simulation conditions described in Table 1, for different box side lengths l.

of SIAs by loops is negligible.

2.2. Cluster dynamics without dispersion of sink strengths

The OKMC simulation of SIA agglomeration is reproduced by CD simulations using the CRESCENDO code [6]. The following equations are solved:

$$\frac{\mathrm{d}C_n}{\mathrm{d}t} = \beta_{n-1}C_{n-1}C_1 - \beta_n C_n C_1 \qquad n \geq 2 \tag{4}$$

$$\frac{\mathrm{d}C_1}{\mathrm{d}t} = \frac{G}{V_{\mathrm{at}}} - \beta_1 C_1 C_1 - \sum_{n\geq 1} \beta_n C_n C_1, \tag{5}$$

where C_n is the concentration of clusters containing n SIAs and $\beta_n C_1$ is the absorption rate of SIAs by these clusters. The sink strength of clusters of size n is defined by

$$k_n^2 = \frac{\beta_n}{D_1} C_n, \tag{6}$$

where D_1 is the diffusivity of SIAs, which means that the loss rate of SIAs, by unit volume, to clusters of size n is

$$\phi_n = k_n^2 D_1 C_1. \tag{7}$$

Temperature	$T = 300\,\mathrm{K}$	
Material: pure aluminum		
Lattice parameter	$a_0 = 0.405\,\mathrm{nm}$	[19]
Atomic volume	$V_{\mathrm{at}} = 1.66\ 10^{-2}\,\mathrm{nm}^3$	
Poisson's ratio	$\nu = 0.35$	[17]
Shear modulus	$\mu = 25.91$ GPa	
SIA properties		
Relaxation volume (for elastic interactions)	$\Delta V = 2.35\,V_{\mathrm{at}}$	[17]
Diffusion prefactor	$5\ 10^{-6}\,\mathrm{m}^2.\mathrm{s}^{-1}$	[19]
Migration energy	$0.105\,\mathrm{eV}$	[19]
Point defect radius	$r_{\mathrm{PD}} = 0.1503$ nm	
SIA loop properties		
Norm of the Burgers vector	$b = 0.2338$ nm	

Table 1: Parameters for the OKMC and CD simulations of SIA agglomeration. The relaxation volume is used in CD, it corresponds to the elastic dipole at stable point used in OKMC, which was computed by density function theory calculations (see Ref. [17]).

We also define the absorption efficiency by

$$\kappa_n = k_n^2 / C_n. \tag{8}$$

Various expressions for sink strengths, or equivalently absorption efficiencies, exist in the literature, especially when the absorption occurs on a sphere. We consider three of them:

- "Laplace" expression [20]:

$$\kappa_n = 4\pi r_n, \tag{9}$$

  where $r_n = r_{\mathrm{L},n} + r_{\mathrm{PD}}$. This formula is derived by assuming that the loop is isolated in an infinite medium, *i. e.* the volume fraction is zero.

- Wiedersich expression [20]:

$$\kappa_n = 4\pi r_n \frac{1-\eta^3}{1-\frac{9}{5}\eta+\eta^3-\frac{1}{5}\eta^6}, \tag{10}$$

where $\eta = r_n/R$ and R is the average half-distance between sinks. This distance is determined at each time step of the CD calculation by

$$\frac{1}{\frac{4\pi}{3}R^3} = \sum_{n\geq 2} C_n. \tag{11}$$

This absorption efficiency is obtained by relating the flux to the loop to the average concentration, assuming a homogeneous production rate of defects and zero flux for $r = R$.

- Effective medium approach [14]:

$$\kappa_n = 4\pi r_n \frac{1 + k_{\text{tot}}R}{1 + k_{\text{tot}}(R - r_n)} \left[1 + \frac{k_{\text{tot}}^2(R - r_n)}{6(1 + k_{\text{tot}}R)} \left((3 + k_{\text{tot}}R)(R + r_n) - 2k_{\text{tot}}r_n^2\right)\right], \tag{12}$$

where k_{tot}^2 is the total sink strength:

$$k_{\text{tot}}^2 = \sum_{n\geq 2} k_n^2 = \sum_{n\geq 2} \kappa_n C_n. \tag{13}$$

In practice, κ_n is calculated by iterating until self-consistency is obtained. Starting with Laplace expression for κ_n ($k_{\text{tot}} = 0$), a converged value is obtained in a few iterations. This kind of approach has been used in the context of Ostwald ripening to account for the dependency of growth rate of particles on the particle's volume fraction [13]. A simpler, approximate expression [14], derived from Eq. (12), is also used in the context of irradiation [21, 22], but it will not be considered here.

Using the same parametrization as for OKMC (Table 1), the cluster size distributions obtained in CD are compared to the OKMC distribution, with $G = 10^{-1}\,\text{dpa.s}^{-1}$ and $t = 10^{-3}\,\text{s}$, in Fig. 2 (a). In OKMC simulations, point defects are absorbed when they enter the encapsulating sphere, which is the same absorption condition as in CD with the three above-mentioned sink strengths.

These results illustrate the fact that the OKMC distributions are broader than the CD ones, whatever the sink strength model. With the Laplace model, the density and mean radius are close to the ones obtained in OKMC, but the distribution is less spread. With the Wiedersich model, which takes into

account the effect of the loop density, a difference with the OKMC distribution is still observed. This model overestimates the mean radius. The effective medium approach also includes the effect of the surrounding environment on the sink strength, but fails to reproduce the OKMC distribution. Even though the average loop radius is less overestimated than with the Wiedersich model, the distribution is not as broad as the OKMC distribution. Similar but less pronounced discrepancies were obtained for lower doses (lower values of G) [18]. These results indicate that taking into account only the average effect of particle volume fraction on sink strength is probably not sufficient to reproduce OKMC results. Sink strength dispersion also needs to be included in the CD formalism.

2.3. Calculations of sink strengths values

In order to calculate the sink strengths of loops in the OKMC microstructures, the previously obtained microstructures are frozen: loops do not grow when SIAs are absorbed and SIAs do not form new loops. Once created, an SIA diffuses in the matrix until it is absorbed by a loop. It is then removed from the simulation and the number of SIAs absorbed by this loop is incremented. The aim of this procedure is to evaluate the loss rate of SIAs to the different sinks of the microstructure, which is directly related to the sink strength.

In practice, a given number M of simulation boxes containing microstructures of loops are selected, typically 10 boxes for each value of G, and the new simulation step begins. The SIA creation rate, noted Γ in this context, is set to ensure a sufficiently large number of point defects in each box at steady state (typically 50 point defects). The average number $\overline{N}_1$ of SIAs is calculated as an average over time and over the boxes. The number N_i^{abs} of SIAs absorbed by each loop i, during the simulation time t, is recorded. The simulated time is chosen to ensure good statistics. The point defect loss rate φ_i to the loop i is then given by

$$\varphi_i = \frac{N_i^{\mathrm{abs}}}{t}. \tag{14}$$

Following Eq. (7), the sink strength of each loop is then calculated according to

$$k_i^2 = \frac{\varphi_i}{D_1 \overline{N}_1}. \tag{15}$$

The sink strength is therefore defined with respect to a global SIA concentration, in agreement with its definition in the CD formalism. From the sink strength values k_i^2, we compute the absorption efficiency κ_i according to (see Eq. (8))

$$\kappa_i = \frac{k_i^2}{1/l^3}, \tag{16}$$

where l is the edge length of the cubic simulation box. We note that since φ_i is the point defect loss rate to a single loop i, the concentration of loops which has to be used in Eq. (8), to define κ_i (a quantity attached to a single sink), is $1/l^3$. It is not the concentration of all loops which have the same size as i, *i.e.* of the class corresponding to i.

The values computed in the microstructures obtained with $G = 10^{-1}$ dpa.s^{-1} and $t = 10^{-3}$ s are presented in Fig. 2 (b). They are compared to the sink strength models previously mentioned, which were used to obtain the CD cluster distributions (Fig. 2 (a)).

The sink strength values obtained in the microstructures are dispersed: loops having the same radius can have very different sink strengths. The values are globally lower than the value given by the Wiedersich model, but can also be below the value given by the Laplace model. The dispersion of sink strength values for loops of same radius but with different environments clearly indicates an environmental effect. We will show in the next sections that this dispersion is responsible for the difference observed on the cluster size distributions.

Similar results were obtained for lower values of G [18]. In that case, the loop density is lower, and the dispersion is also less important. Thus, it seems that the dispersion is reduced when the sink density diminishes. To illustrate this fact on comparable microstructures, the simulation boxes studied above are dilated to reduce the loop density. The box dimensions and distances between the loops are increased while the loops radii are preserved. The absorption efficiencies obtained for different densities are shown in Fig. 3. It is clear from

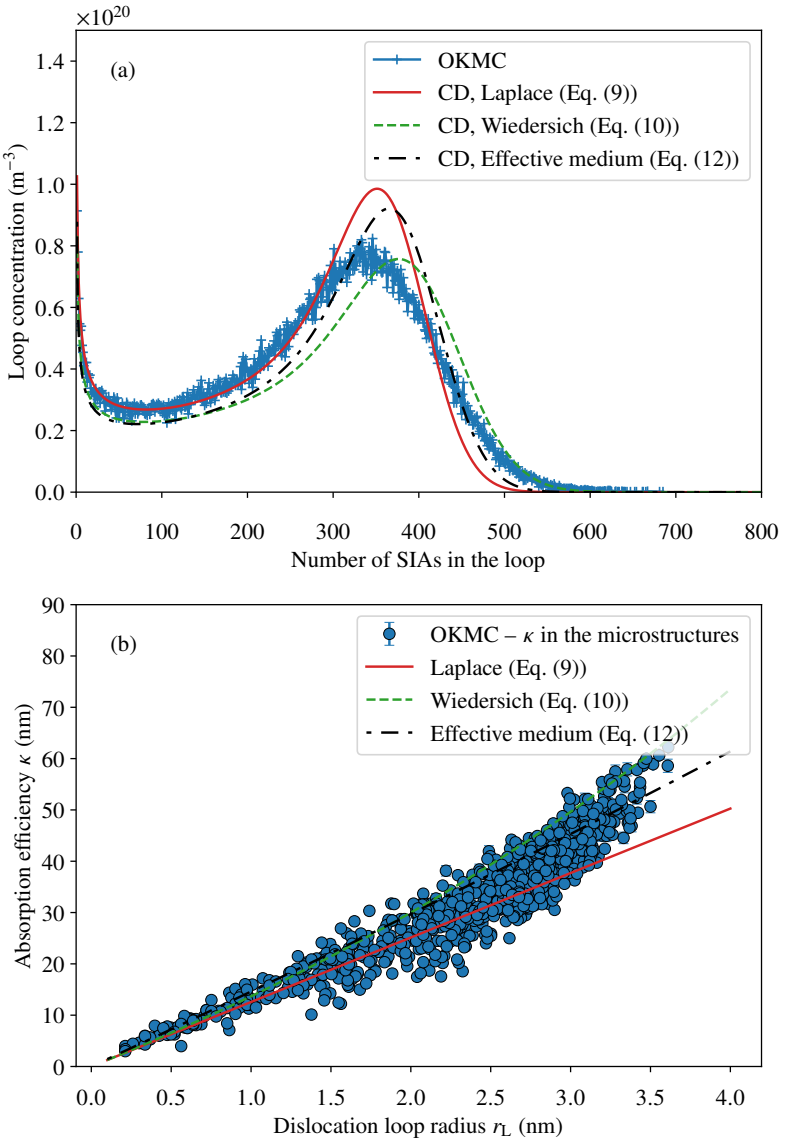

Figure 2: (a) Cluster size distributions obtained from OKMC simulations and equivalent CD simulations, using various sink strength models (see text), obtained with $G = 10^{-1}\,\mathrm{dpa.s}^{-1}$ and $t = 10^{-3}\,\mathrm{s}$. (b) Absorption efficiencies calculated for the loops in the OKMC microstructures and sink strength models used in CD.

this figure that the dispersion increases with the loop density.

3. A model to represent sink strength dispersion

To analyze the correlation between the sink strength value and the environment of loops, we determine the Voronoi cells of all loops in OKMC microstructures, using the QHULL program [23]. The Voronoi cell of a loop contains all points which are nearer to the loop than to any other loop. It gives a first appraisal of the local environment around a loop: the sink density around a loop increases as the volume of the Voronoi cell of the loop decreases.

Results for the microstructures obtained in OKMC with $G = 10^{-1}\,\mathrm{dpa.s^{-1}}$ and $t = 10^{-3}\,\mathrm{s}$ are shown in Fig. 4. They unveil a correlation between the volumes and the sink strength values: loops with higher sink strengths tend to have bigger Voronoi volumes. Similar results are obtained for other simulated doses, especially for lower values of G [18]. One can also see in Fig. 4 that the bigger loops tend to be in bigger cells. This can be understood by the mechanism of loop growth: a loop in a big cell has no loop in its close neighborhood. Hence, it can grow more rapidly. Inversely, a big loop easily absorbs neighboring mobile point defects, preventing any loop nucleation in its neighborhood, so its Voronoi cell remains large. The correlation between the sink strength and the Voronoi volume is however not perfect. Indeed, we checked that the sink strength values are also influenced by the shape of Voronoi cells and the loop position in its cell [18]. However, the cell size remains the prevalent effect in the cases considered here.

The Voronoi volumes therefore seem to be key elements to understand the sink strength dispersion. In order to be able to use these parameters as input data for CD calculations, the distributions of normalized Voronoi volumes in the OKMC microstructures are calculated. The results are shown in Fig. 5 at different times, for $G = 10^{-1}\,\mathrm{dpa.s^{-1}}$. They are compared to the so-called "Poisson-Voronoi distribution", which refers here to the distribution of volumes obtained for a Voronoi tessellation of points randomly distributed in space. An

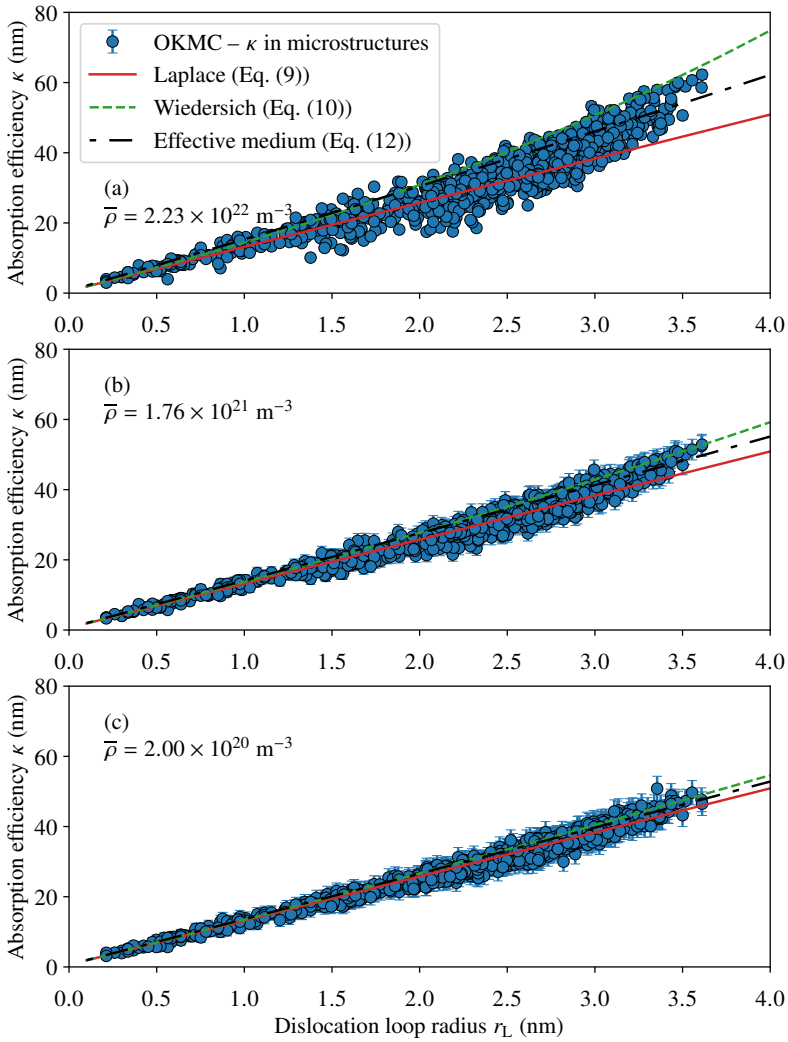

Figure 3: (a) Absorption efficiencies calculated in the OKMC microstructures obtained with $G = 10^{-1}$ dpa.s^{-1} and $t = 10^{-3}$ s, loop density of $\overline{\rho} = 2.23\ 10^{22}$ m^{-3} ($l = 200$ nm) (b) Absorption efficiencies obtained in dilated boxes ensuring a loop density of $\overline{\rho} = 1.76\ 10^{21}$ m^{-3} ($l = 466$ nm) (c) Absorption efficiencies obtained in dilated boxes ensuring a loop density of $\overline{\rho} = 2.00\ 10^{20}$ m^{-3} ($l = 962$ nm). The error bars represent the statistical error [18], they are displayed on all data.

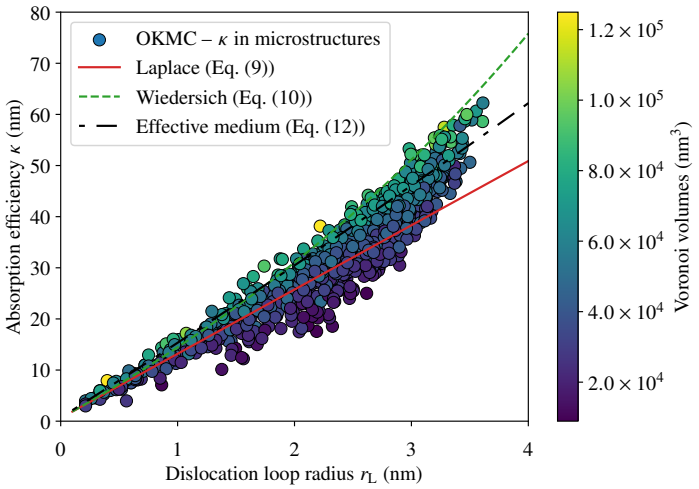

Figure 4: Correlations between the absorption efficiencies and Voronoi volumes (colorbar). Values are obtained in OKMC microstructures with a creation rate of $G = 10^{-1}$ dpa.s^{-1} and for a simulated time of $t = 10^{-3}$ s.

accurate approximation of the Poisson-Voronoi distribution is given by the expression proposed by Kumar *et al.* [24], whose parameters have been determined by Lazar *et al.* [25]. It can be seen that the distribution of normalized Voronoi volumes obtained in OKMC remains unchanged with time and that it is in very good agreement with the Poisson-Voronoi distribution. Therefore, it can be inferred that the loops are randomly distributed in the box. In addition, the expression of Kumar *et al.* can be used to give the distribution of Voronoi volumes, which is the main physical ingredient for sink strength dispersion.

The correlation of sink strengths with Voronoi volumes can be understood the following way. A cluster i in a small Voronoi volume V_i is surrounded by a density of clusters larger than the average density. The local sink strength around i, $k^2_{i,\mathrm{loc}}$, is therefore higher than the average total sink strength k^2_{tot}. Since as a first approximation, the local monomer concentration around i is related to the local sink strength through

$$C_{i,\mathrm{loc}} = \frac{\Gamma}{V_{\mathrm{at}} D_1 k^2_{i,\mathrm{loc}}}, \tag{17}$$

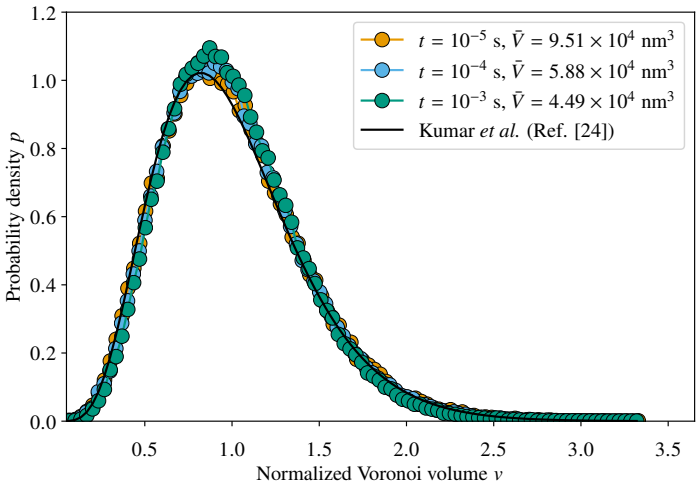

Figure 5: Distribution of normalized volumes of Voronoi cells $v = V/\bar{V}$, where $\bar{V}$ is the average Voronoi volume, at different times, in OKMC microstructures with a creation rate of $G = 10^{-1}\,\mathrm{dpa.s}^{-1}$.

we see that it is lower than the average SIA concentration $\bar{C}$, given by

$$\bar{C} = \frac{\Gamma}{V_{\mathrm{at}} D_1 k_{\mathrm{tot}}^2}. \tag{18}$$

In other words, the local concentration of point defects around sink i is lower than the average concentration because there is a larger number of sinks in its vicinity to absorb point defects. Therefore the loss rate to the sink, which is related to the local concentration of point defects available for absorption, appears to decrease as the Voronoi volume decreases. In the CD mean field formalism, the sink strength relates the loss rate to a sink to the point defect concentration averaged over the whole system ($\bar{C}$, or equivalently, $\overline{N}_1$, see Eq. (15)). It means that for a small Voronoi volume, the low loss rate is equivalent to a low sink strength.

A simple calculation permits to relate more precisely the sink strength to Voronoi volumes. Let φ_i be the loss rate of SIAs to sink i. For a spherical sink, it can be written, to lowest order, as

$$\varphi_i = 4\pi r_i D_1 C_{i,\mathrm{loc}}. \tag{19}$$

Using Eqs. (17) and (18) in Eq. (19) yields

$$\varphi_i = 4\pi r_i D_1 \frac{k_{\text{tot}}^2}{k_{i,\text{loc}}^2} \bar{C}. \tag{20}$$

Assuming that the average radius of clusters surrounding i is $\bar{r}$ and the local volume is $V_{i,\text{loc}}$, the local sink strength is approximately

$$k_{i,\text{loc}}^2 = 4\pi \bar{r} \frac{1}{V_{i,\text{loc}}}. \tag{21}$$

Since $k_{\text{tot}}^2 = 4\pi\bar{r}/\bar{V}$, we finally obtain

$$\varphi_i = 4\pi r_i D_1 \frac{V_{i,\text{loc}}}{\bar{V}} \bar{C}. \tag{22}$$

The local volume V_{loc} associated with each loop remains to be determined. A simple approach is to use the average Voronoi volume of its nearest neighbors. To determine an expression of this volume, a Poisson-Voronoi tessellation of 10^5 points is generated. For each Voronoi cell of volume V_i, the average volume of nearest neighbors is calculated (Fig. 6). Nearest neighbor cells are defined as neighbors which share a face. The average volume of neighbors is well fitted by the following expression:

$$\frac{V_{\text{loc}}}{\bar{V}} = \left(\frac{V}{\bar{V}}\right)^{\alpha} + \beta, \tag{23}$$

with $\alpha = 0.25$ and $\beta = 0.07$. It is not clear if the volume itself should be included in the average. In principle it affects the local concentration, so taking it into account may be more correct. As shown in the figure, including it marginally impacts the average volume, due to the large number of neighbors [26]. In the following this contribution will not be considered.

The normalized local volumes $V_{\text{loc}}/\bar{V}$ have also been extracted from the OKMC simulations, using Eq. (22). They are displayed in Fig. 7 as a function of normalized Voronoi volumes $v = V/\bar{V}$, for $G = 10^{-1}\,\text{dpa.s}^{-1}$. These OKMC results are in good agreement with Eq. (23). OKMC values are still dispersed around the analytical formula. This dispersion comes from the fact that sink strengths not only depend on Voronoi volume, but also on the shape of the Voronoi cell and the sink position in its cell [18].

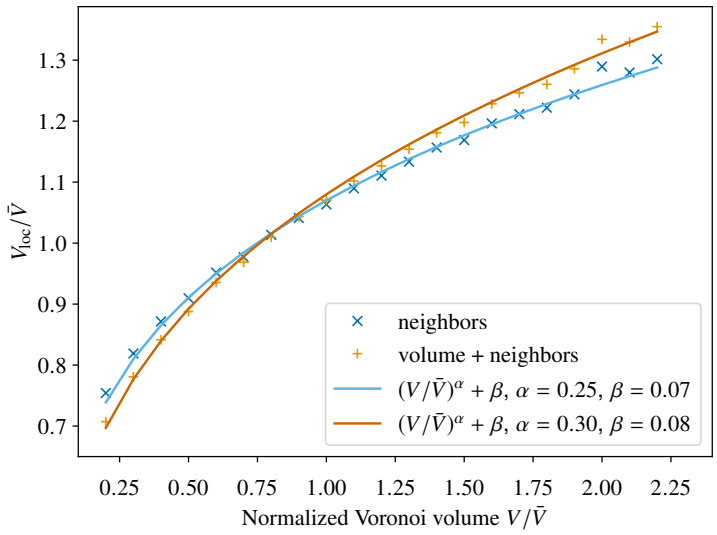

Figure 6: Average Voronoi volume of neighbors in a Poisson-Voronoi tessellation (blue symbols). For the orange symbols, the cell itself is included in the average. The distribution contains 10^5 Voronoi volumes.

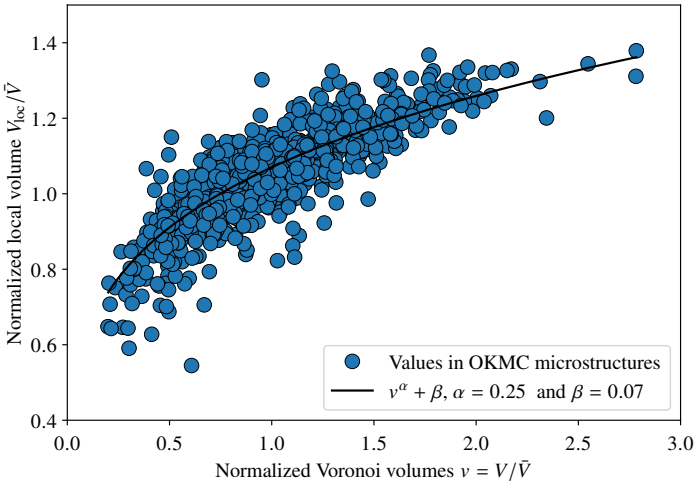

Figure 7: Values of normalized local volumes $V_{i,\mathrm{loc}}/\bar{V}$ (see text) obtained in OKMC microstructures, as a function of the normalized Voronoi volume.

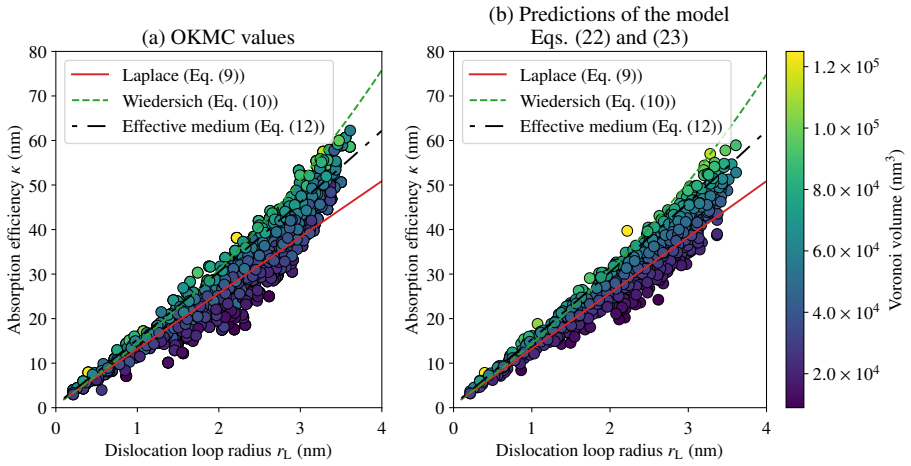

Figure 8: (a) Absorption efficiencies calculated in the OKMC microstructures obtained with $G = 10^{-1}$ dpa.s^{-1} and $t = 10^{-3}$ s. (b) Absorption efficiencies calculated from the loop radii and Voronoi volumes using Eqs. (22) and (23).

Finally, for the conditions $G = 10^{-1}$ dpa.s^{-1} and $t = 10^{-3}$ s, absorption efficiencies calculated by OKMC and predicted by Eqs. (22) and (23), using the Voronoi volumes from OKMC simulations, exhibit almost identical distributions (Fig. 8). This means that Voronoi cell shape and sink position in Voronoi cell are probably second order effects compared to the volume of the Voronoi cell itself, when we focus on the sink strength. We note, however, that since the sink strength dispersion is observed to increase with density, the proposed approach tends to overestimate the dispersion for low sink densities and to underestimate it for large sink densities.

To summarize, the absorption efficiencies in the microstructures can be reproduced by the expression

$$\kappa = 4\pi r \frac{V_{\text{loc}}}{\bar{V}}, \tag{24}$$

where V_{loc} is the average Voronoi volume of loops in the neighborhood. It depends on the Voronoi volume of the loop according to Eq. (23), with $\alpha = 0.25$ and $\beta = 0.07$. The normalized Voronoi volume $V/\bar{V}$ follows the distribution corresponding to a Poisson-Voronoi tessellation. An analytical form of this

distribution is given by Kumar *et al.* [24], and the parameters can be found in Ref. [25].

4. Introducing sink strength dispersion in cluster dynamics simulations

In previous sections we characterized the sink strength dispersion and derived an expression to reproduce this dispersion, based on the distribution of Voronoi volumes. Now we introduce the sink strength dispersion in the classical CD equations (4) and (5). To do so, the absorption coefficient β_n is assumed to depend on the normalized Voronoi volume v for a size larger than n^*, with $n^* \geq 2$:

$$\beta_n(v) = 4\pi r_n \left(v^\alpha + \beta\right) D_1. \tag{25}$$

The cluster concentration of a given class n now also depends on v, so it is noted $C_n(v)$. As reported in Section 2, large clusters are present more frequently in large Voronoi cells than in small ones. This means that the change of neighborhood of a cluster, or in other words the change of its Voronoi cell, due to the creation of a cluster nearby, must happen over timescales which are sufficiently large with respect to the growth process. Accordingly, we do not include any coupling term between $C_n(v)$ and $C_n(v')$: the neighborhood of a cluster is assumed to remain the same. Therefore a cluster in a large Voronoi volume, whose sink strength is large, remains in a large Voronoi volume. In reality, depending on the irradiation conditions, some clusters may nucleate in its vicinity, leading to a reduction of its Voronoi volume and of its sink strength. This approximation can be checked a posteriori on cluster distributions.

Equations (4)–(5) become

$$\frac{\mathrm{d}C_n}{\mathrm{d}t} = \beta_{n-1}C_{n-1}C_1 - \beta_n C_n C_1 \qquad 2 \leq n \leq n^* - 1 \tag{26}$$

$$\frac{\mathrm{d}C_n(v)}{\mathrm{d}t} = P(v)\beta_{n-1}C_{n-1}C_1 - \beta_n(v)C_n(v)C_1 \qquad n = n^*,\ v \in]0, \infty[\tag{27}$$

$$\frac{\mathrm{d}C_n(v)}{\mathrm{d}t} = \beta_{n-1}(v)C_{n-1}(v)C_1 - \beta_n(v)C_n(v)C_1 \qquad n > n^*,\ v \in]0, \infty[\tag{28}$$

$$\frac{\mathrm{d}C_1}{\mathrm{d}t} = -\beta_1 C_1 C_1 - \sum_{1 \leq n \leq n^*-1} \beta_n C_n C_1 - \int_0^\infty \sum_{n \geq n^*} \beta_n(v) C_n(v) C_1 P(v)\, \mathrm{d}v. \tag{29}$$

In these equations, $P(v)$ is the Poisson-Voronoi distribution in normalized Voronoi volumes.

To solve these equations numerically, two methods can be used. The first one consists in discretizing the values of v, so concentrations can be noted $C_{n,i} = C_n(v_i)$, where $i = 1, \ldots, N$ and N is the number of equally spaced possible normalized Voronoi volumes (see Fig. A.14 in Appendix A). The numerical cost can increase substantially, since the number of equations is roughly multiplied by N compared to a classical calculation involving a single population. A more elegant way to solve equations (26)–(29) is to resort to a hybrid deterministic-stochastic scheme recently developed for cluster dynamics equations [27]. In this method, small clusters ($n < n^*$) are treated deterministically, while cluster dynamics equations are solved stochastically for larger sizes. The deterministic and stochastic regions are separated by a buffer region where the transfer between deterministic cluster density and stochastic particles is performed. Sink strength dispersion can be naturally introduced in this method. Each time a stochastic particle is created, due to the flux of clusters from the deterministic region to the stochastic region, a normalized Voronoi volume, drawn in the Poisson-Voronoi distribution, is associated to this particle. The particle then evolves according to the value of the absorption coefficient corresponding to the normalized Voronoi volume. To ensure good performance and accuracy of the hybrid algorithm, the deterministic region must contain at least a few tens of classes. Here, n^* is set to 20.

Results are compared to OKMC simulations for $t = 10^{-3}$ s, $t = 2\ 10^{-3}$ s and $t = 10^{-2}$ s for the highest dose rate ($G = 10^{-1}$ dpa.s^{-1}), which corresponds to the highest cluster density (Figs. 9 and 10; see Supplementary Material for the case $G = 10^{-3}$ dpa.s^{-1} and $t = 10^{-2}$ s). The fully deterministic calculations with dispersion were performed with $N = 50$. It was checked, by varying this value, that in the conditions considered the cluster distributions are accurately simulated. For too low values of N ($N \lesssim 30$), cluster distributions become distorted at the largest dose. Two values for n^* were considered in these calculations: $n^* = 2$ and $n^* = 20$. The latter corresponds to the value used in the hybrid method.

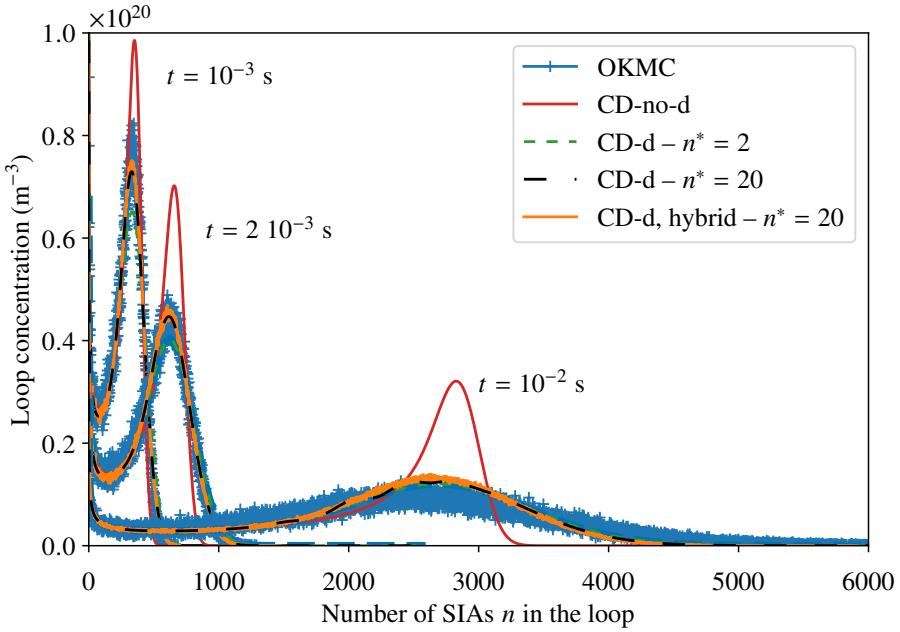

Figure 9: Cluster distributions at $t = 10^{-3}$ s, $t = 2\ 10^{-3}$ s and $t = 10^{-2}$ s, obtained with OKMC and different CD models: deterministic calculation without dispersion and Laplace expression for sink strengths (CD-no-d), deterministic calculation with sink strength dispersion based on Eqs. (A.1)–(A.4) with $N = 25$ and two values for n^* (CD-d), hybrid deterministic-stochastic calculation using sink strength dispersion in the stochastic region (CD-d, hybrid). Hybrid calculations were performed with 2 million stochastic particles.

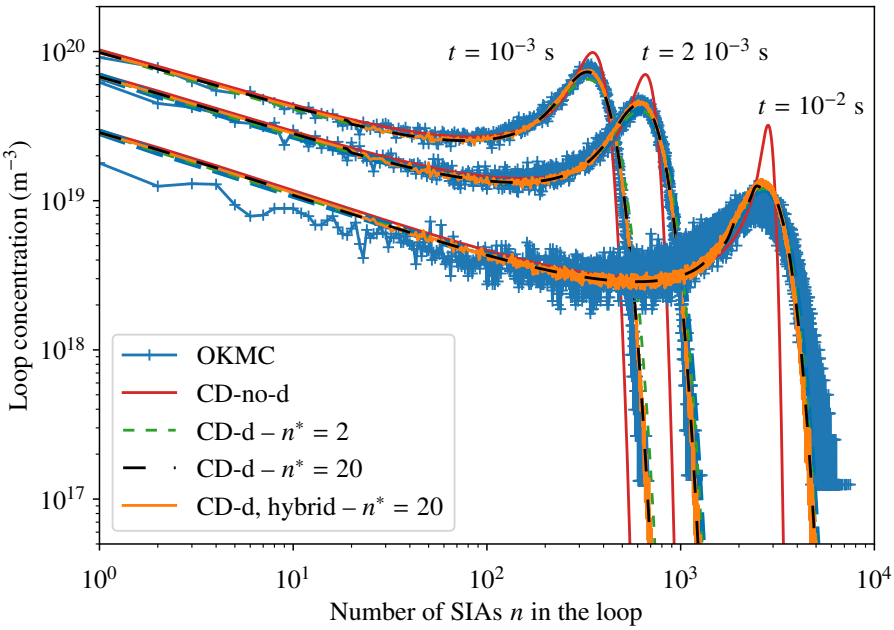

Figure 10: Cluster distributions at $t = 10^{-3}$ s, $t = 2\ 10^{-3}$ s and $t = 10^{-2}$ s, obtained with OKMC and different CD models, in logarithmic scale. See Fig. 9 for more information.

We first see that the results obtained with the hybrid and the deterministic solving, for $n^* = 20$, perfectly match, which validates the two numerical methods. However, the large number of equations to solve deterministically at high doses ($\sim 5 \times 10^5$) makes the deterministic method computationally intensive, so the hybrid method should be preferred. CD calculations including sink strength dispersion are all in much better agreement with OKMC than is the classical CD calculation using Laplace expression for sink strengths, which leads to excessively peaked distributions. To compare more quantitatively the agreement between CD and OKMC distributions, we calculate the "distance" between CD and OKMC distributions $\tilde{C}^{\mathrm{CD}}$ and $\tilde{C}^{\mathrm{OKMC}}$ by using the L^2 norm:

$$\left\| \tilde{C}^{\mathrm{CD}} - \tilde{C}^{\mathrm{OKMC}} \right\| = \sqrt{\sum_{n \geq 2} \left(C_n^{\mathrm{CD}} - C_n^{\mathrm{OKMC}} \right)^2}. \tag{30}$$

The ratio of the distance involving the CD distributions with sink strength dispersion to that involving the standard CD distributions without dispersion is 0.32, 0.21 and 0.33 at times $t = 10^{-3}$ s, $t = 2\ 10^{-3}$ s and $t = 10^{-2}$ s, respectively. This shows that at all times the improvement is significant. Distributions obtained with $n^* = 2$ are slightly broader than with $n^* = 20$, due to the larger number of classes where dispersion is present. However, this difference tends to decrease with time, since the flux of clusters in the region of cluster space containing small clusters becomes lower (the nucleation rate decreases).

At short time ($t = 10^{-3}$ s), especially for $n^* = 2$, the CD cluster distributions are broader than the OKMC distributions. As discussed previously, sink strength dispersion increases with cluster density (so with time) and Eq. (23) with $\alpha = 0.25$ and $\beta = 0.07$ reproduces well the dispersion for $t = 10^{-3}$ s, but overestimates the dispersion for shorter times. This overestimation can explain why the distributions are slightly too broad. The choice $n^* = 20$, due to numerical constraints in the hybrid method, improves the agreement with OKMC results. This is due to the fact that no dispersion is taken into account for $n < n^*$, which compensates for the overestimation of dispersion at short times. At $t = 2\ 10^{-3}$ s, the discrepancy with OKMC increases if no dispersion is taken into account, whereas CD simulations including dispersion remain very

close to OKMC. Finally, if the calculation is continued up to $t = 10^{-2}$ s, we see that CD cluster distributions without sink strength dispersion are far too peaked, whereas distributions with sink strength dispersion tend to be slightly narrower than OKMC distributions. Here again, this is due to the absence of dependence of Eq. (23) on cluster density. Despite this limitation, the overall good agreement for times $t = 2\ 10^{-3}$ s and $t = 10^{-2}$ s is rather encouraging concerning the generality of the approach, inasmuch as no data were fitted at these times. In the following, we use the hybrid approach and thus we consider only calculations with $n^* = 20$.

The absorption efficiencies of the stochastic particles κ is shown in Fig. 11 as a function of the cluster radius, for $t = 10^{-3}$ s. The overall shape of the distribution is very similar to the one in Fig. 2 (b), with large clusters mostly present in large Voronoi cells. This is consistent with the fact that clusters with large Voronoi cells grow faster and that the environment of particles does not change with time in CD calculations. The similarity of sink strength distributions in CD and OKMC validates this approximation. A more refined model could be envisaged, by resampling some of the absorption rates of stochastic particles depending on the nucleation rate of clusters. For the present case, this additional complexity proved to be unessential.

5. Extension to toroidal geometry and effect of elastic interactions

The aim of this part is to show that the new CD formulation can be extended to a more realistic situation in which absorption by a loop is realized on a torus and in which elastic effects are taken into account. SIAs are absorbed on the torus of radius $r_{\mathrm{L},n}$ (see section 2.1). Using the same method as previously described, we determine the cluster size distributions, with or without the strain fields generated by the loops. The strain field of loops can be taken into account in OKMC simulations using the method described in [17], and the analytical strain field expression given in [28, 29]. Values of elastic dipole tensors determined in Ref. [17] by density functional theory calculations at stable and

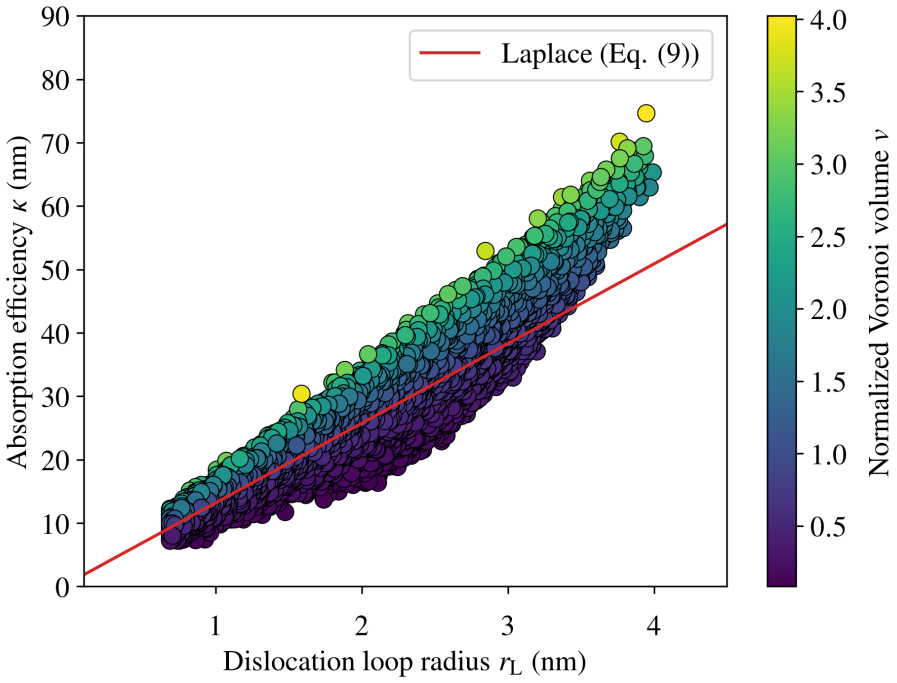

Figure 11: Normalized sink strengths at $t = 10^{-3}$ s, extracted from the values ascribed to stochastic particles in CD hybrid calculations.

saddle positions are used in the present OKMC simulations.

The corresponding CD models used here are described in Ref. [15]. When the strain fields are neglected, the absorption can be represented by expression (18) of Ref. [15], combined with expression (17) of Ref. [15] to include the effect of non-zero volume fraction. To take into account the strain fields, the pipe radius is replaced by an effective radius $r_{\mathrm{p}}^{\mathrm{eff}}$ depending on the material and point defect properties, according to expressions (19) and (20) of Ref. [15]. In this expression SIAs are considered to be isotropic defects with the same relaxation volume at stable and saddle points (see Table 1).

The cluster size distributions obtained in OKMC are compared to the corresponding CD distributions in Fig. 12, for an SIA creation rate of $G = 10^{-1}$ dpa.s^{-1} and a simulated time of $t = 10^{-3}$ s. The first thing to note is the large influence of elastic interactions on the cluster distributions. As for the spherical clusters studied above, one can see that the OKMC distributions are wider than the CD ones when no dispersion is taken into account.

The same analysis of the sink strengths in OKMC microstructures has been performed, and similar results were obtained regarding the sink strength dispersion and Voronoi volume distributions. To reproduce the sink strength dispersion, we use the same approach as the one described above. In agreement with what was done for the absorption on spheres, we choose to disperse the values of sink strengths around the value for the infinite medium. The absorption efficiency reads:

$$\kappa = 2\pi r_{\mathrm{L}} Z^{\mathrm{loop}} \frac{V_{\mathrm{loc}}}{\bar{V}}, \tag{31}$$

where V_{loc} is given by Eq. (23), and Z^{loop} is defined in Ref. [15] and depends on r_{p} if strain fields are neglected or $r_{\mathrm{p}}^{\mathrm{eff}}$ if they are taken into account.

Following section 4, the dispersion is introduced in CD using the absorption coefficient β_n, which reads

$$\beta_n = 2\pi r_{\mathrm{L},n} Z^{\mathrm{loop}} \left(v^{\alpha} + \beta\right) D_1. \tag{32}$$

The results obtained using this model are shown in Fig. 12. As for the case of spherical clusters, the introduction of dispersion in CD leads to a much better

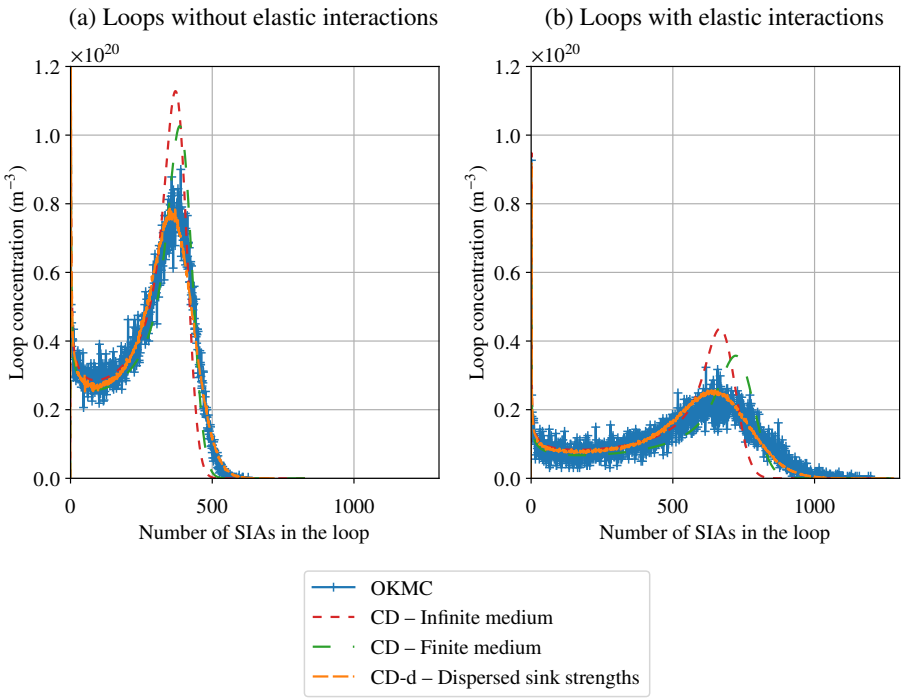

Figure 12: Cluster size distributions obtained when the absorption occurs on the dislocation line (a) without elastic interactions and (b) with elastic interactions. The CD models without dispersion are given in Ref. [15] (see text).

agreement with OKMC distributions. Therefore the proposed method can be extended to more realistic systems, assuming that the absorption occurs on the torus and taking into account the effect of elastic interactions.

6. Comparison between experimental and simulated loop distributions

The effect of sink strength dispersion on cluster distributions has been tested up to limited doses (10^{-3} dpa) because we wanted to compare the CD results to reference cluster distributions obtained by OKMC simulations. In this section, we describe CD simulations to much higher doses (1 dpa). Since no comparison can be made with OKMC in this case, simulations are compared to experimental measurements of cluster distributions. Results obtained by Chen *et al.* [30] for dislocation loops in aluminum thin foils were chosen for several reasons. In this experiment, the damage was produced by electron irradiation. Under these conditions, only Frenkel pairs are generated, so point defect clusters are created by the successive agglomeration of point defects. Frenkel pair accumulation is known to be more easily simulated than displacement cascade conditions with mean field CD [31, 32], especially at high doses where cascade overlap occurs. The foils considered in the experiment by Chen *et al.* are relatively thick (around 500 nm), which, here again, is relatively favorable for mean field approaches. Finally, cluster distributions are provided at several times. This permits to determine some simulation parameters with more confidence. While comparing simulations to experiments, it should be kept in mind that rather large bins (5 nm on loop diameter) were used to determine the cluster distributions experimentally.

Equations used to simulate the experiments are based on Eqs. (4) and (5) (Eqs. (26)-(29) if the dispersion of sink strengths is taken into account). In addition, vacancies and vacancy clusters are taken into account. Single vacancies can be absorbed by point defect clusters and recombine with SIAs. Point defects can also be absorbed by surfaces. Emission of point defects by point defect

clusters is taken into account in the model. However, the binding energies of point defects to dislocation loops are so high that at the temperature considered, emission can be neglected. Although vacancy clusters are included in the model for the sake of generality, they do not form since the di-vacancy is not stable [33], so they do not play any role in the simulations. A more detailed description of the equations can be found, for example, in Ref. [6].

In the simulations, surfaces are taken into account by a specific sink term [34], for the sake of simplicity and computational efficiency. Such an approach leads to similar results as spatialized calculations [35], but avoids to perform averages of cluster distributions over the depth to make a comparison with experiments, which could introduce artificial oscillations in the distributions' shape if the number of slices was too low. The initial dislocation density is set to zero, since micrographs show the absence of dislocations in the region of observation before irradiation [30]. The temperature is set to 300 K. Based on a displacement cross-section of 15 barns [36], the damage rate is estimated to 3×10^{-4} dpa.s^{-1}. It has been shown by Chen *et al.* that the production of defects depends on the orientation of the foil, the $\langle 111 \rangle$ direction being one where it is the highest. In addition, the fraction of freely migrating defects (FMDs) is not precisely known. Only FMDs must be taken into account in CD models, since other defects quickly recombine with each other and do not participate to loop growth. Therefore, there is some uncertainty on the production rate of defects to use in CD. We chose a fraction of FMDs equal to one, to reflect the high production rate of defects along $\langle 111 \rangle$ direction and the probably small proportion of close pairs in this material [30]. This means that the actual creation rate of SIAs and vacancies in the model is 3×10^{-4} dpa.s^{-1}. More work at atomic scale would be necessary to determine the damage rate precisely, but this is beyond the scope of this application.

Experiments were first simulated with the deterministic CD model described in Ref. [15] (Eqs. 18 – 20) and used in the previous section, without sink strength dispersion. Some parameters were adjusted to obtain a reasonable agreement with the experimental densities and average sizes of loops (Tab. 2).

The saturation in loop density observed after 10 min of irradiation indicates that loop nucleation has stopped at this time. This behavior is not observed if the recommended value for the vacancy migration energy (0.61 eV, see Ref. [19]) is taken. A slightly higher value must be adopted to increase the vacancy concentration and suppress loop nucleation from a certain time, *i. e.* the system must enter the recombination regime. The value 0.7 eV has been adopted. The migration energy of SIAs has also been increased to 0.19 eV, to produce loop densities similar to the experimental values. The recommended value (0.11 eV) produces far too low cluster densities. These two parameter modifications may point to an effect of impurities, as suggested in the experimental study. Finally, the relaxation volume of the vacancy was changed from -0.4 V_{at} [19] to -0.8 V_{at}. The resulting increase of the elastic interactions between vacancies and loops may reflect the effect of saddle point anisotropy of vacancies on the sink strength [17]. This anisotropy has been shown to increase significantly the sink strength of loops [18].

Loop distributions are shown at three different times in Fig. 13. As discussed previously, although the densities and average sizes are correctly reproduced, cluster distributions obtained experimentally and with CD without sink strength dispersion are markedly different. Experimental distributions are much broader.

Simulations were also performed with the new formalism, which includes the effect of sink strength dispersion. This effect was taken into account for the absorption of both SIAs and vacancies. Since the sink strength dispersion only depends on Voronoi volumes, which are not related to the properties of the absorbed defect, the approach is the same for vacancies as for SIAs.

Introducing the sink strength dispersion slightly shifts the peak position to larger sizes, since the average value of $V_{\mathrm{loc}}/\bar{V}$ in Eq. (23) does not equal 1 (it is the case for $\beta = 0.01687$). It also significantly broadens the distribution and improves the agreement with experiments, which shows the importance of taking into account the dispersion. The ratio of distances between cluster distributions (see Eq. (30)) is 0.47, 0.43 and 0.31 at 15, 30 and 60 min. Although a clear improvement is obtained, the agreement with experimental results is still not

Parameter	Value	Reference
Temperature	300 K	
Damage rate	3×10^{-4} dpa s^{-1}	
Thickness of the foil	500 nm	
Network dislocation density	0	
Lattice parameter	0.405 nm	
Diffusion prefactor for vacancies	10^{-5} m^2 s^{-1}	[19]
Diffusion prefactor for SIAs	5×10^{-6} m^2 s^{-1}	[19]
Migration energy of vacancies	0.7 eV	adjusted
Migration energy of SIAs	0.19 eV	adjusted
Relaxation volume of SIAs	1.9 V_{at}	[19]
Relaxation volume of vacancies	-0.8 V_{at}	adjusted
Recombination radius	$2a_0$	[37]
Binding energy of two vacancies	0	[33]
Binding energy of two SIAs	0.8 eV	

Table 2: Parameters for CD simulations of electron irradiation of aluminum thin foils.

perfect. Among the possible sources of discrepancy, the absence of dependence of Eq. (23) on cluster density is a probable one. Trends are consistent with the fact that CD distributions with sink strength dispersion tend to be slightly narrower than OKMC distributions at the largest simulated dose ($t = 10^{-2}$ s, see Figs. 9 and 10). Other sources of discrepancy include the simplified treatment of the effect of vacancy anisotropy at saddle position on the sink strength, effects of impurities which have been taken into account in an effective way and surface effects. Even if the foil thickness is large, surfaces may have some effects on the loop distributions which are not properly handled in mean field calculations. In particular, our analysis on Voronoi volume implicitly assumes that the considered sink is surrounded by other sinks, which is not the case when it is close to a surface. Larger spreading of growth rates may arise because of the presence of this additional sink.

7. Discussion

In the previous sections we have shown that it is possible to obtain a good agreement between CD results and OKMC results at high volume fraction, provided that the sink strength dispersion is introduced in CD. This dispersion is primarily due to the variation of local sink density around sinks. To our knowledge, sink strength dispersion has not been much studied for microstructures obtained under irradiation; however, there is a vast amount of theoretical and experimental results for the effect of local surroundings in Ostwald ripening. In this context, most of the works have focused on much higher volume fractions (of the order of percent or more) and theoretical works have introduced a dependency of the particle's average growth rate on volume fraction (for a review, see Ref. [10]). Although some laws can be transposed to the microstructures under irradiation (see for example Refs. [13] and [14]), the simulation of Ostwald ripening has its own peculiarities. Evolution of particles is due to the Gibbs-Thomson effect, so the dependency of the growth rate on local surroundings can result not only from different local densities, but also from different particle's

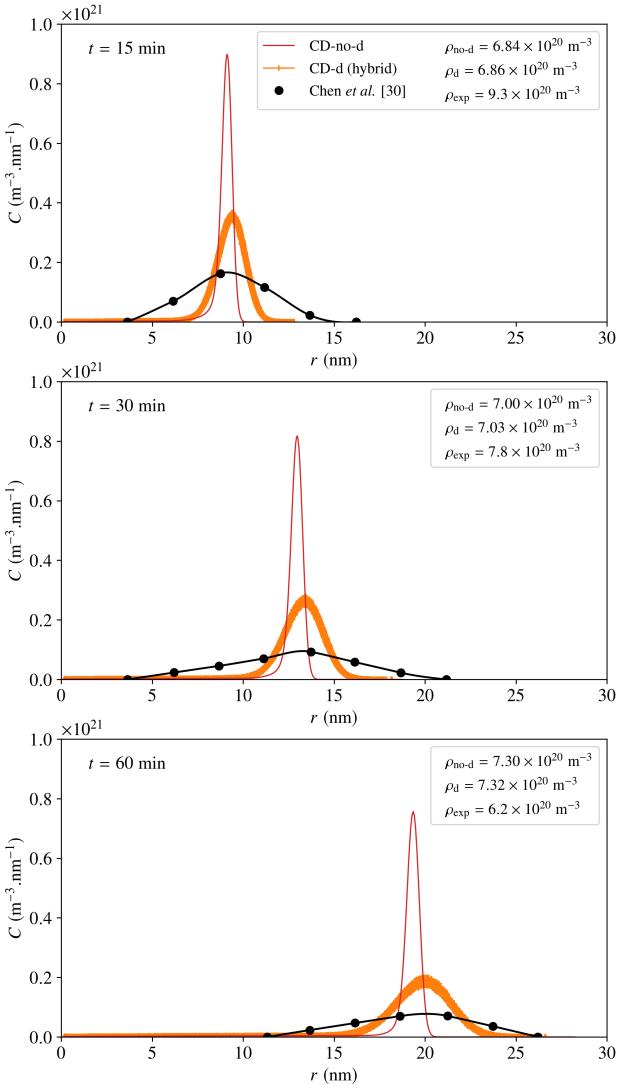

Figure 13: Experimental and simulated loop distributions for electron irradiated aluminum thin foils at different times. CD simulations are performed without (CD-no-d) and with (CD-d) sink strength dispersion. Loop densities $\rho_{\text{no-d}}$, ρ_{d} and ρ_{exp} are shown at each time.

radii. Under irradiation, at sufficiently low temperature, the large supersaturation makes Gibbs-Thomson effect negligible. Both effects (local density and particule radius) are included in the sink strength dispersion highlighted in the simulation of Ostwald ripening (see Fig. 4 in Ref. [11]), but their respective contribution remains unknown. In the case of microstructures produced under irradiation, we have seen that introducing only the average effect of volume fraction, as it is done classically for Ostwald ripening, is not sufficient: the sink strength dispersion must also be included. The large effect of local density on the particle's growth rate seems rather surprising, compared to the simulations of Ostwald ripening. More in-depth investigation would be needed to explain these seemingly different results.

The inability of models based only on volume fraction-dependent average growth rate to reproduce OKMC cluster distributions is visible in Fig. 2. One of these models (effective medium), proposed by Brailsford *et al.* [14], is shown in this figure. Although the average values measured by OKMC reasonably agree with this law, the associated cluster distributions are markedly different. Sink strengths obtained by OKMC can even be lower than the Laplace solution, which is below the values given by the volume fraction-dependent laws. The inability of these laws to reproduce such dispersed data explains why cluster distributions obtained with OKMC are much broader than those obtained using standard CD. We have chosen to introduce dispersion around the Laplace law, since it fairly represents the average value of the sink strengths for all cases considered in this study and it can be efficiently implemented in CD. Additional data should be collected, especially at larger doses, to see if this choice is always relevant.

To ensure that the correction is general, more complex cases should be considered. For example, the dispersion is assumed to be independent of the volume fraction. Fig. 3 shows, however, that the dispersion tends to increase with volume fraction. In addition, we have only considered one type of defect in our simulations where OKMC and CD are compared. A more realistic case would be to consider vacancies and SIAs at the same time. Concerning vacancies, our model including elastic interactions remains to be tested: analytical expressions

for sink strengths all rely on the description of defects as isotropic defects with the same relaxation volume at stable and saddle points [38, 39, 15]. Although this approximation is deemed correct for SIAs, it may be too crude for vacancies which are highly anisotropic at saddle position. It may be one of the reasons of the remaining discrepancy between our simulations and experiments by Chen *et al.* [30] reported in Section 6. As discussed in this section, additional sinks such as surfaces and grain boundaries may also change the sink strength dispersion of clusters if their density is appreciable.

8. Conclusion

Using a combination of CD and OKMC simulations, we have studied the effect of local surroundings on particle size distributions for microstructures under irradiation. Distributions obtained by OKMC are shown to be broader than those simulated by CD, even if the average effect of finite volume fraction is introduced in the sink strengths used in CD. We have shown that the sink strength dispersion must be included in CD in order to reproduce OKMC results. To come to this conclusion, we used a two-step procedure:

- Simple laws for the sink strengths were proposed to reproduce the sink strength dispersion measured with OKMC in realistic microstructures. These laws depend on the solution in infinite medium (Laplace solution), multiplied by a factor which depends on the Voronoi volume associated with the sink.

- A new formalism of CD was developed in order to integrate the sink strength dispersion. Cluster classes not only depend on the cluster size, but also on the normalized Voronoi volume of the cluster.

Using this new approach, we showed that it is possible to obtain a satisfactory agreement between the cluster distributions simulated by CD and OKMC in all cases considered, although CD distributions become slightly narrower at the largest doses. A comparison was then made with experimental dislocation

loop distributions obtained by electron irradiation of aluminum thin foils up to 1 dpa. It was shown that the agreement is much better with sink strength dispersion than without, but that differences still exist. Sources for this residual discrepancy were discussed. More complex cases, involving for example two kinds of point defects and the presence of other sinks, should now be considered.

Acknowledgments

This study was partially funded by the SIMMAT project from the I3P institute (CEA-EDF R&D). It has received funding from the Euratom research and training program 2014-2018 under Grant Agreement N°661913. CRESCENDO code is co-developed in collaboration with EDF R&D within the framework of I3P institute.

Data availability

The relevant data are available within the article or from the authors upon reasonable request.

Appendix A. Deterministic solving of the CD equations including sink strength dispersion

The deterministic solving of Eqs. (26)–(29) can be done by discretizing the values of v (Fig. A.14), noted v_i, where $i = 1, \ldots, N$ and N is the number of equally spaced possible normalized Voronoi volumes. Values v_i between 0 and 5 are sufficient to accurately sample the Poisson-Voronoi distribution (Fig. 5). The spacing between two values of v is noted Δv. We use the notations $\beta_{n,i} = \beta_n(v_i)$

and $P_i = P(v_i)$. This leads to the set of equations to solve:

$$\frac{\mathrm{d}C_n}{\mathrm{d}t} = \beta_{n-1}C_{n-1}C_1 - \beta_n C_n C_1 \qquad 2 \leq n \leq n^* - 1 \tag{A.1}$$

$$\frac{\mathrm{d}C_{n,i}}{\mathrm{d}t} = \Delta v P_i \beta_{n-1}C_{n-1}C_1 - \beta_{n,i}C_{n,i}C_1 \qquad n = n^*,\ i \in [1, N] \tag{A.2}$$

$$\frac{\mathrm{d}C_{n,i}}{\mathrm{d}t} = \beta_{n-1,i}C_{n-1,i}C_1 - \beta_{n,i}C_{n,i}C_1 \qquad n > n^*,\ i \in [1, N] \tag{A.3}$$

$$\frac{\mathrm{d}C_1}{\mathrm{d}t} = -\beta_1 C_1 C_1 - \sum_{1 \leq n \leq n^*-1} \beta_n C_n C_1 - \sum_{i=1}^{N} \Delta v P_i \sum_{n \geq n^*} \beta_{n,i} C_{n,i} C_1. \tag{A.4}$$

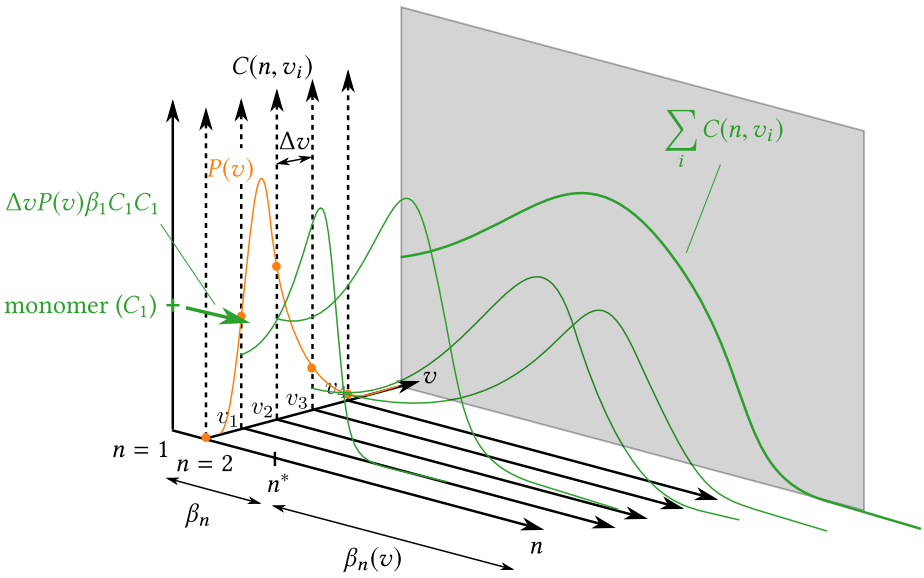

Figure A.14: Schematics of the deterministic solving of CD equations including sink strength dispersion.

This set of equations can be readily introduced in the CD code CRESCENDO, which enables the use of different cluster populations coupled together only through the mobile species [6]. Here, the different cluster populations actually correspond to the same clusters, but in different environments.

References

[1] M. H. Mathon, A. Barbu, F. Dunstetter, F. Maury, N. Lorenzelli, C. H. de Novion, J. Nucl. Mater. 245 (1997) 224.

[2] E. Clouet, A. Barbu, L. Lae, G. Martin, Acta Mater. 53 (2005) 2313.

[3] T. Jourdan, F. Soisson, E. Clouet, A. Barbu, Acta Mater. 58 (2010) 3400.

[4] S. I. Golubov, B. N. Singh, H. Trinkaus, Philos. Mag. A 81 (2001) 2533.

[5] A. Hardouin-Duparc, C. Moingeon, N. Smetniansky-de-Grande, A. Barbu, J. Nucl. Mater. 302 (2002) 143.

[6] T. Jourdan, G. Bencteux, G. Adjanor, J. Nucl. Mater. 444 (2014) 298.

[7] J. Lépinoux, Philos. Mag. 86 (2006) 5053.

[8] J. Lépinoux, C. Sigli, Philos. Mag. 93 (2013) 3194.

[9] T. Jourdan, J.-P. Crocombette, Comput. Mater. Sci. 145 (2018) 235.

[10] P. W. Voorhees, J. Stat. Phys. 38 (1985) 231.

[11] P. W. Voorhees, M. E. Glicksman, Acta Metall. 32 (1984) 2013.

[12] I. Rovelli, S. L. Dudarev, A. P. Sutton, J. Mech. Phys. Solids 103 (2017) 121.

[13] A. D. Brailsford, P. Wynblatt, Acta Metall. 27 (1979) 489.

[14] A. D. Brailsford, R. Bullough, M. R. Hayns, J. Nucl. Mater. 60 (1976) 246–256.

[15] T. Jourdan, J. Nucl. Mater. 467 (2015) 286.

[16] C. Domain, C. S. Becquart, L. Malerba, J. Nucl. Mater. 335 (2004) 121.

[17] D. Carpentier, T. Jourdan, Y. Le Bouar, M.-C. Marinica, Acta Mater. 136 (2017) 323.

[18] D. Carpentier, Simulation of the absorption kinetics of point defects by dislocations and defect clusters, Ph.D. thesis, Université Paris-Saclay, 2018.

[19] P. Ehrhart, Atomic defects in metals · Al: Datasheet from Landolt-Börnstein - Group III Condensed Matter · Volume 25: "Atomic Defects in Metals" in SpringerMaterials (http://dx.doi.org/10.1007/10011948_58), 1991.

[20] F. A. Nichols, J. Nucl. Mater. 75 (1978) 32.

[21] L. Malerba, C. S. Becquart, C. Domain, J. Nucl. Mater. 360 (2007) 159.

[22] T. Ahlgren, L. Bukonte, J. Nucl. Mater. 496 (2017) 66.

[23] C. B. Barber, D. P. Dobkin, H. T. Huhdanpaa, ACM Trans. Math. Softw. 22 (1996) 469.

[24] S. Kumar, S. K. Kurtz, J. R. Banavarn, M. G. Sharma, J. Stat. Phys. 67 (1992) 523.

[25] E. A. Lazar, J. K. Mason, R. D. MacPherson, J. D. Srolovitz, Phys. Rev. E 88 (2013) 063309.

[26] A. Thorvaldsen, Mater. Sci. Forum 94-96 (1992) 307.

[27] P. Terrier, M. Athènes, T. Jourdan, G. Adjanor, G. Stoltz, J. Comput. Phys. 350 (2017) 280.

[28] T. A. Khraishi, J. P. Hirth, H. M. Zbib, M. A. Khaleel, Int. J. Eng. Sci. 38 (2000) 251.

[29] F. Kroupa, Czech. J. Phys. B 10 (1960) 284.

[30] J. H. Chen, P. Rao, P. S. Ho, Radiat. Eff. 18 (1973) 157.

[31] T. Jourdan, J.-P. Crocombette, Phys. Rev. B 86 (2012) 054113.

[32] A. Y. Dunn, L. Capolungo, Comp. Mater. Sci. 102 (2015) 314.

[33] H. Wang, D. Rodney, D. Xu, R. Yang, P. Veyssière, Phys. Rev. B 84 (2011) 220103.

[34] R. Bullough, M. R. Hayns, M. H. Wood, J. Nucl. Mater. 90 (1980) 44.

[35] A. Barbu, C. S. Becquart, J.-L. Bocquet, J. Dalla Torre, C. Domain, Philos. Mag. 85 (2005) 541.

[36] O. S. Oen, Cross sections for atomic displacements in solids by fast electrons, Technical Report ORNL-4897, ORNL, 1973.

[37] W. G. Wolfer, A. Si-Ahmed, J. Nucl. Mater. 99 (1981) 117.

[38] W. A. Coghlan, M. H. Yoo, in: M. F. Ashby, R. Bullough, C. S. Hartley, J. P. Hirth (Eds.), Dislocation Modelling of Physical Systems, Pergamon, 1981, pp. 152–157.

[39] V. I. Dubinko, A. S. Abyzov, A. A. Turkin, J. Nucl. Mater. 336 (2005) 11.

Supplementary material for "Effect of sink strength dispersion on cluster size distributions simulated by cluster dynamics"

D. Carpentier[1], T. Jourdan[1], P. Terrier[1,2], M. Athènes[1], and Y. Le Bouar[3]

[1]*DEN-Service de Recherches de Métallurgie Physique, CEA, Université Paris-Saclay, F-91191, Gif-sur-Yvette, France*
[2]*Université Paris-Est, CERMICS (ENPC), INRIA, F-77455 Marne-la-Vallée, France*
[3]*LEM, Université Paris-Saclay, ONERA, CNRS, 29 av. de la division Leclerc, 92322 Châtillon, France*

In this supplementary material we present the cluster distributions obtained with a lower damage rate ($G = 10^{-3}$ dpa.s^{-1}), in the case of the absorption on spheres without elastic interactions. The reference distribution could not be obtained with OKMC due to CPU time constraints, so event-based kinetic Monte Carlo (EKMC) was used instead. This method does not permit to take into account elastic interactions but in the conditions considered here, it is faster than OKMC and yields identical results.

The same results as in the article are obtained (Fig. S1). The cluster distribution without sink strength dispersion (CD-no-d) is too peaked. Introducing sink strength dispersion through our hybrid approach (CD-d) leads to a much better agreement with the reference calculation.

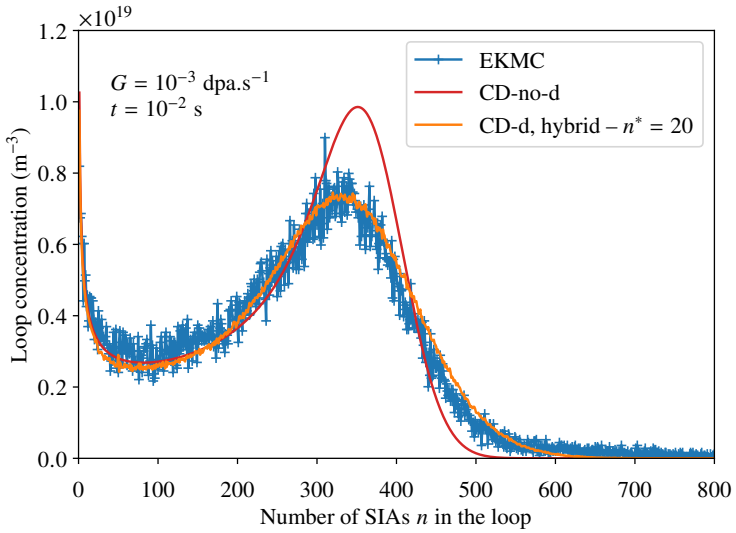

FIG. S1: Cluster distributions at $t = 10^{-2}$ s, obtained with EKMC and two different CD models: deterministic calculation without dispersion and Laplace expression for sink strengths (CD-no-d), hybrid deterministic-stochastic calculation using sink strength dispersion in the stochastic region (CD-d).